
The Journal of Immunology

# Novel Role of TRPML2 in the Regulation of the Innate Immune Response

Lu Sun, Yinan Hua, Silvia Vergarajauregui, Heba I. Diab and Rosa Puertollano

*J Immunol* 2015; 195:4922-4932; Prepublished online 2 October 2015;
doi: 10.4049/jimmunol.1500163
http://www.jimmunol.org/content/195/10/4922



*The Journal of Immunology* is published twice each month by
The American Association of Immunologists, Inc.,
1451 Rockville Pike, Suite 650, Rockville, MD 20852

Print ISSN: 0022-1767 Online ISSN: 1550-6606.

# Novel Role of TRPML2 in the Regulation of the Innate Immune Response

**Lu Sun,[1] Yinan Hua,[1] Silvia Vergarajauregui, Heba I. Diab, and Rosa Puertollano**

**TRPMLs (or mucolipins) constitute a family of endosomal cation channels with homology to the transient receptor potential superfamily. In mammals, the TRPML family includes three members: TRPML1–3. Although TRPML1 and TRPML3 have been well characterized, the cellular function of TRPML2 has remained elusive. To address TRPML2 function in a physiologically relevant cell type, we first analyzed TRPML2 expression in different mouse tissues and organs and found that it was predominantly expressed in lymphoid organs and kidney. Quantitative RT-PCR revealed tight regulation of TRPML2 at the transcriptional level. Although TRPML2 expression was negligible in resting macrophages, TRPML2 mRNA and protein levels dramatically increased in response to TLR activation both in vitro and in vivo. Conversely, TRPML1 and TRPML3 levels did not change upon TLR activation. Immunofluorescence analysis demonstrated that endogenous TRPML2 primarily localized to recycling endosomes both in culture and primary cells, in contrast with TRPML1 and TRPML3, which distribute to the late and early endosomal pathway, respectively. To better understand the in vivo function of TRPML2, we generated a TRPML2-knockout mouse. We found that the production of several chemokines, in particular CCL2, was severely reduced in TRPML2-knockout mice. Furthermore, TRPML2-knockout mice displayed impaired recruitment of peripheral macrophages in response to i.p. injections of LPS or live bacteria, suggesting a potential defect in the immune response. Overall, our study reveals interesting differences in the regulation and distribution of the members of the TRPML family and identifies a novel role for TRPML2 in the innate immune response.** ***The Journal of Immunology*****, 2015, 195: 4922–4932.**

Transient receptor potential (TRP) channels constitute a large family of cation channels involved in a variety of physiological functions, particularly sensory signaling (1, 2). TRPs share a common topology of six-membrane-spanning helices with both the N- and C-terminal tails oriented toward the cytosol and the pore located between transmembrane segments five and six. The TRP superfamily is divided into seven subfamilies, one being the mucolipin subfamily (also known as TRPML) (3, 4). In mammals, the TRPML family includes three members (TRPML1, TRPML2, and TRPML3) that share ~75% amino acid similarity.

Mutations in TRPML1 cause mucolipidosis type IV (5–7), an autosomal recessive disease characterized by mental and psychomotor retardation, diminished muscle tone (hypotonia), decreased gastric acid (achlorhydria), and visual problems, including corneal clouding, retinal degeneration, sensitivity to light, and strabismus (8–12). Meanwhile, a gain-of-function mutation in TRPML3 results in the murine varitint-waddler phenotype, which is characterized by hearing loss, vestibular dysfunction (circling behavior, head bobbing, waddling), and coat color dilution (13). In contrast, no clinically significant mutation in TRPML2 has been reported.

TRPMLs display some unique properties. Although most TRPs function at the cell surface, responding to changes in the extracellular environment, TRPMLs localize to endo/lysosomal organelles. Specifically, TRPML1 localizes primarily to late endosomes/lysosomes (14–16). Several groups suggested that TRPML1-mediated release of intralysosomal calcium is critical in regulating lysosomal fusion with different intraorganellar compartments, including autophagosomes (17), phagosomes (18), and the plasma membrane (19, 20). TRPML1 also was implicated in lysosomal acidification (21), lysosomal iron release (22), and zinc homeostasis (23). In contrast to the ubiquitous distribution of TRPML1, high levels of TRPML3 expression appear to be restricted to specific cell types, including melanocytes, hair cells of the inner ear, and neonatal enterocytes (24, 25). TRPML3 distributes at the plasma membrane, as well as the earlier compartments of the endocytic pathway (early and late endosomes) (26, 27). Overexpression of TRPML3 causes severe alterations in the endosomal pathway, including enlargement and clustering of endosomes, delayed epidermal growth factor receptor degradation, and impaired autophagosome maturation (26, 27). In addition, inhibition of TRPML3 function results in increased accumulation of endosomal luminal calcium, impaired endosomal acidification, and aberrant endosome fusion (28).

Although the channel properties and function of TRPML1 and TRPML3 are well established, those of TRPML2 are far less characterized. Work in *drosophila* S2 cells revealed that the TRPML2 channel displays nonselective cation permeability, which is $Ca^{2+}$ permeable and inhibited by low extracytosolic pH (29). Also, quantitative RT-PCR analysis showed that TRPML2 mRNA is expressed at a very low level in most organs, with the exception of thymus, spleen, and, to a lesser degree, kidney (30).

Cell Biology and Physiology Center, National Heart, Lung, and Blood Institute, National Institutes of Health, Bethesda, MD 20892

[1]L.S. and Y.H. contributed equally to this work.

Received for publication January 22, 2015. Accepted for publication September 10, 2015.

This work was supported by the Intramural Research Program of the National Institutes of Health, National Heart, Lung, and Blood Institute.

Address correspondence and reprint requests to Dr. Rosa Puertollano, Cell Biology and Physiology Center, National Heart, Lung, and Blood Institute, National Institutes of Health, 9000 Rockville Pike, Building 50/3537, Bethesda, MD 20892. E-mail address: puertolr@mail.nih.gov

The online version of this article contains supplemental material.

Abbreviations used in this article: Ad-TRPLM2, adenovirus encoding untagged mouse TRPML2; BM, bone marrow; BMDM, BM-derived macrophage; ES, embryonic stem; ETEC, enterotoxigenic *Escherichia coli*; KO, knockout; LB, Luria–Bertani; NHLBI, National Heart, Lung, and Blood Institute; TFE3, transcription factor E3; TFEB, transcription factor EB; TfR, transferrin receptor; TRP, transient receptor potential; WT, wild-type.

www.jimmunol.org/cgi/doi/10.4049/jimmunol.1500163

The lack of reliable Abs against endogenous TRPML2 has complicated the study of the intracellular distribution of this protein. Our group reported that heterologously expressed TRPML2 mainly localized to Arf6-regulated recycling endosomes in HeLa cells (31). Moreover, expression of a TRPML2 dominant-negative mutant significantly impaired the recycling of internalized GPI-anchored proteins back to the plasma membrane (31).

In this study, we sought to better understand the physiological function of TRPML2 in vivo. We first analyzed the expression of TRPML2 in different tissues and cell types and found that the levels of TRPML2 are dramatically upregulated in macrophages upon TLR activation. Generation of a TRPML2-knockout (KO) mouse confirmed a novel role for TRPML2 in the innate immune response.

## Materials and Methods

### *Mice and tissue preparation*

C57BL/6, C57BL/6-Cre mice were purchased from The Jackson Laboratory (Bar Harbor, ME). To generate TRPML2-KO mice, we purchased mouse embryonic stem (ES) cells containing the *Trpml2*$^{tm1e(KOMP)Wtsi}$ allele (clone EPD0300_5_B06) from the University of California, Davis Knockout Mouse Project Repository. This nonconditional potential allele has a trapping cassette SA-βgeo-pA (splice acceptor–β-geo–polyA) flanked by flippase recombinase target FRT sites upstream of exon 4, resulting in truncation of the endogenous transcript and, thus, creating a constitutive null mutation. The cassette also tags the gene with a lacZ reporter. The FRT flanked region is followed by a promoter-driven neo cassette that is floxed by two loxP sites and can be further removed by the Cre recombinase to achieve a clean KO. The ES cells were injected into C57BL/6 blastocysts. These blastocysts were then implanted into the uterus of Swiss-Webster female mice to complete the pregnancy. Chimeric mice were born and crossed with B6 albino for offspring that are all black. These black mice are heterozygous and inbred to produce TRPML2-KO mice.

Mice were genotyped by long-range PCR following the protocol of International Knockout Mouse Consortium project 37138 (http://www.mousephenotype.org/martsearch_ikmc_project/martsearch/ikmc_project/37138). The two primer pairs used were LAR3 5′-CAC AAC GGG TTC TTC TGT TAG TCC-3′ and GF3 5′-CTC TGA GTT CGT AAG CGA GCG AGC-3′; and RAF5 5′-CAC ACC TCC CCC TGA ACC TGA AAC-3′ and GR3 5′-GAA GAG AGC ATC AGA ATA CTT GGA CAA CAG-3′. After successful identification of TRPML2-KO mice, the colony was maintained by genotyping using the following primer mix for PCR: FRT-F 5′-GTA TAG GAA CTT CGT CGA GAT AAC-3′, M2-5F 5′-CTC AGT GAA CCA AGG AAG GAG AGG-3′, and M2-3R 5′-CTC ATA TGT GGT CCC TTG GCT CTT-3′.

*Trpml2* $^{flox\text{-}frt\text{-}neo/flox\text{-}frt\text{-}neo}$ mice were crossed with EIIA-Cre mice (The Jackson Laboratory) to facilitate an in vivo *neo* deletion that generated final clean *Trpml2*-KO mice. The neo cassette–deleted mice were genotyped by two primer pairs: 5′-CAC TTG CTG ATG CGG TGC TGA TTA C-3′ and 5′-GAC ACC AGA CCA ACT GGT AAT GGT AG-3′, and, M2-5F 5′-CTC AGT GAA CCA AGG AAG GAG AGG-3′ and M2-3R 5′-CTC ATA TGT GGT CCC TTG GCT CTT-3′. TRPML2 KOs were confirmed by quantitative RT-PCR with mouse TRPML2 probes (QT00133434) (QIAGEN, Valencia, CA) to detect TRPML2 mRNA expression.

All of the mice were bred and/or maintained in the National Heart, Lung, and Blood Institute (NHLBI) specific pathogen–free animal facility. Experiments were performed when mice were 8 to 14 wk of age under protocols approved by the NHLBI Animal Care and Use Committee.

### *Macrophage stimulation in vivo and in vitro*

LPS from *Escherichia coli* 0127:B8 was obtained from Sigma (St. Louis, MO; cat. no. L3129) and dissolved in saline solution at 100 ng/μl. The LPS solution was sterilized and injected i.p. at a dose of 0.5 μg/g of body weight. At the indicated times, peritoneal cells were harvested by rinsing the peritoneal cavity with 6 ml HBSS. After washing, cells were stained for FACS experiments or lysed for mRNA and protein assessments.

For in vivo macrophage activation with live bacteria, enterotoxigenic *Escherichia coli* (ETEC) strain H10407 was purchased from the American Type Culture Collection (Manassas, VA; ATCC 35401) and grown overnight in Luria–Bertani (LB) broth at 37–C. Bacteria were pelleted, washed twice in sterile PBS, diluted to 200 μl sterile PBS containing $5 \times 10^7$ CFU, and injected i.p. into wild-type (WT) and TRPML2-KO mice. The actual CFU was confirmed by a serial dilution test on an LB agar plate.

RAW 264.7 cells were cultured in DMEM plus 10% FBS. MH-S cells were cultured in RPMI 1640 with 10% FBS. At the indicated times, cultured cells were stimulated with 1 μg/ml LPS or 0.2 μg/ml R848 (Enzo Life Sciences, Farmingdale, NY).

### *Cell culture and in vitro differentiation*

To obtain bone marrow (BM)–derived macrophages (BMDMs), BM cells were isolated from femurs and tibias of 8-wk-old female mice. Suspended BM cells were cultured in BM-differentiation medium: RPMI 1640 supplemented with 10% FBS, 100 U/ml penicillin, 100 μg/ml streptomycin, 2 mM L-glutamine, and 40 ng/ml recombinant murine M-CSF (PeproTech, Rocky Hill, NJ). Cells were seeded in non–tissue culture–treated Petri dishes (BD351029) and incubated at 37˚C in a 5% $CO_2$ atmosphere. Four days after seeding, fresh BM-differentiation medium was added to each plate, and cells were incubated for an additional 3 d. To isolate BMDMs, supernatants were discarded, and attached cells were washed with sterile HBSS. Macrophages were detached by adding 2 ml cell stripper (Invitrogen) and incubated at 37˚C for 5 min.

Alveolar macrophages were obtained by digesting isolated mouse lung tissue with Liberase (0.14 U/ml; Roche) at 37˚C for 60 min. After digestion, separated cells were washed with RPMI 1640 with 20% FBS and plated onto 10-cm culture dishes (BD350003) with 20 ml RPMI 1640 containing 20% FBS for 7 d. Medium was changed on day 2. The alveolar macrophages were loosely attached on fibroblast cells and harvested by pipetting with a 1-ml tip.

Microglia cells were extracted from P1 mouse brains. Every four dissected cortices were placed in 15-ml conical tubes with 10 ml ice-cold HBSS for 30 min. After aspirating HBSS, brains were triturated and digested with 4 ml trypsin/EDTA at 37˚C for 15 min. The enzymatic digestion was stopped by adding 4 ml complete microglial media (DMEM with 10% FBS, 0.08% gentamicin). The cells were centrifuged at 1500 rpm for 5 min, resuspended in 10 ml microglial complete media, and plated on a 10-cm tissue culture dish coated with poly-D-lysine. Medium was changed on day 3, and cells were harvested on day 10.

RAW 264.7 cells (ATCC) were maintained in DMEM plus 10% FBS. They were split every 3 d. MH-S cells (ATCC) were cultured in RPMI 1640 with 10% FBS. Passage procedure was identical to that of RAW 264.7 cells. All cell lines were incubated at physiologic levels (37˚C, 5% $CO_2$).

### *Adenovirus*

Adenovirus expressing mouse TRPML2 was prepared, amplified, and purified by Welgen.

### *Flow cytometry*

Cell suspensions were preincubated with an Ab specific for mouse FcγII/III (2.4G2; Harlan) for 10 min on ice. Cells were stained on ice for 15 min with a mixture of fixable viability dye (eBioscience, San Diego, CA) and with fluorochrome-conjugated mAbs against several surface markers, including CD11b (M1/70), F4/80 (BM8), CD80 (16-10A1), MHC class I (AF6-88.5.5.3), Ly-6G (Gr-1), and CD16/CD32 (eBioscience, San Diego, CA). Flow cytometry data were collected with an LSR II flow cytometer system (BD Biosciences, San Jose, CA), and the results were analyzed using FlowJo software (TreeStar). Peritoneal macrophages were recognized as double positive for CD11b and F4/80. Based on fluorescence intensity, these macrophages included two populations: the resident macrophages (bright for both CD11b and F4/80) and recruited macrophages (dim for the same markers). Peritoneal neutrophils were recognized as double positive for Ly-6G and CD16.

### *RNA isolation and quantitative RT-PCR*

RNA was isolated from cells using the PureLink Total RNA Purification System (Invitrogen, Carlsbad, CA), following the manufacturer's recommendations. RNA yield was quantified by measuring the OD at 260 and 280 nm using an Eppendorf BioPhotometer. One microgram RNA was reverse transcribed in a 20-μl reaction using oligo(dT)20 and SuperScript III First-Strand Synthesis System (Invitrogen), following the manufacturer's recommendations. PCR was performed using 5 μl SYBR GreenER qPCR SuperMix (Invitrogen), 2 μl cDNA, 1 μl gene-specific primer mix (QuantiTect primer Assays; QIAGEN), and 2 μl water, for a total reaction volume of 10 μl. Quantification of gene expression was performed using the 7900HT Fast Real-Time PCR System (Applied Biosystems, Carlsbad, CA). The thermal profile of the reaction was 50˚C for 2 min, 95˚C for 10 min, and 40 cycles of 95˚C for 15 s followed by 60˚C for 1 min. All samples were run in triplicates. Amplification of the sequence of interest was compared with a reference probe (mouse β-actin,

QT01136772) and normalized against a standard curve of cell line mRNA. The 7900HT Fast Real-Time PCR System Software was used for data analyses (Applied Biosystems).

### *Western blotting*

Lysates were collected by resuspending cells in lysis buffer (25 mm HEPES-KOH [pH 7.4], 250 mm NaCl, 1% Triton X-100 (w/v) supplemented with protease inhibitor mixture), passing them through a 25-gauge needle, and collecting soluble fractions after centrifugation. Samples were analyzed by SDS-PAGE (4–20% gradient gels) under reducing conditions and transferred to nitrocellulose. Membranes were immunoblotted using the indicated Abs. HRP chemiluminescence was developed using Western Lightning Chemiluminescence Reagent Plus (PerkinElmer Life Sciences, Bridgeville, PA).

TRPML2 Ab was generated by injecting GST-N terminal TRPML2 (39 aa) fusion protein into rabbits (Pierce, Rockford, IL) and purified from day-72 bleeding serum. The DNA sequence coding the mouse TRPML2 N-terminal 39 aa was amplified by PCR. The primers used were 5′-AAT AAT GGA TCC TCA TGC CCG GAG ACG AG-3′ and 5′-ATT ATG CGG CCG CTC ACT CTT CCC TCA CCT C-3′. The PCR was digested by restriction enzyme and inserted into a PGEX-5X1 vector BamHI/NotI site. The plasmid construct was transfected into Rosetta 2 (Millipore, Billerica, MA)–competent cells, and GST fusion protein was induced by 100 μM IPTG at 30˚C overnight. The GST-N terminal TRPML2 was purified using Glutathione Sepharose beads (GE Healthcare, Milwaukee, WI) and injected into rabbits. The rabbit serum was sequentially purified by Affi-Gel 10 columns preconjugated with GST and GST-TRPML2 proteins (Bio-Rad, Hercules, CA). Mouse anti-actin was purchased from BD Biosciences.

### *Confocal microscopy*

Macrophages attached to coverslips were fixed in 4% paraformaldehyde and permeabilized with 0.2% Triton X-100 at room temperature for 10 min. Coverslips were then incubated with specific primary Abs diluted in immunostaining solution (0.1% saponin, 1% FBS in PBS) for 1 h at room temperature, followed by incubation with a fluorophore-conjugated secondary Ab for 30 min at room temperature. Mouse TRPML2 was stained with rabbit polyclonal anti-TRPML2 primary Ab, followed by Alexa Fluor 488– or Alexa Fluor 568–labeled Goat anti-Rabbit IgG (Molecular Probes, Eugene, OR). Transferrin receptor was recognized by mouse anti-TfR Ab (clone H68.4; Invitrogen; cat. no. 13-6800), followed by Alexa Fluor 488– or Alexa Fluor 568–labeled goat anti-mouse IgG. LAMP1 was stained first with Rat anti-Mouse LAMP1 (1D4B; Developmental Studies Hybridoma Bank, Iowa City, IA), followed by Alexa Fluor 488–labeled Donkey anti-Rat IgG. Giantin polyclonal Ab was from Covance (PRB-114C), and CCL2 mouse mAb (clone 2D8) was from EMD Millipore

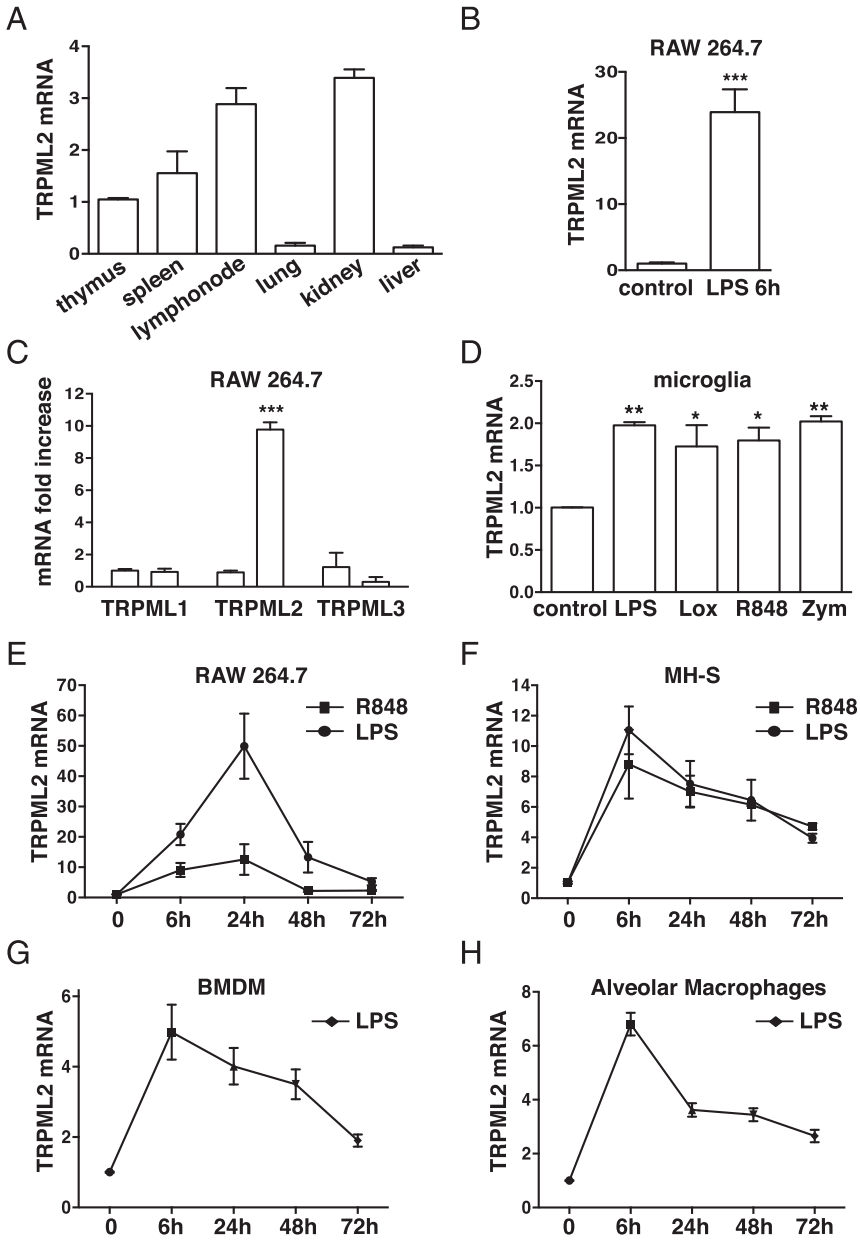


**FIGURE 1.** TRPML2 is transcriptionally upregulated in activated macrophages. (**A**) Measurement of TRPML2 mRNA levels from different C57BL/6N mice organs by quantitative RT-PCR. TRPML2 mRNA levels were normalized to TRPML2 levels in thymus and represent fold change. Data are mean ± SD of four (thymus, liver) or three (spleen, lymph node, lung, kidney) independent experiments. (**B** and **C**) RAW 264.7 cells were left untreated or incubated with 1 μg/ml LPS for 6 h. Cells were collected, and TRPML2 (B) or TRPML1-3 (C) mRNA levels were measured by quantitative RT-PCR ($n$ = 20). (**D**) Transcriptional upregulation of TRPML2 in microglia in response to various TLR activators. Cultured microglia cells were treated with the following reagents for 6 h: LPS (1 μg/ml, TLR4 ligand), loxoribine (100 nM, TLR7 ligand), R848 (200 ng/ml, TLR7 and TLR8 ligand), and zymosan A (50 μg/ml, TLR2 ligand). Data are mean ± SD of three independent experiments. Time course of TRPML2 mRNA levels upon LPS and R848 stimulation for 6 h in RAW 264.7 ($n$ = 14) (**E**) and MH-S ($n$ = 9) (**F**) cells. (**G** and **H**) Time course of TRPML2 mRNA levels in cultured primary macrophages. Data are mRNA fold change for BMDMs ($n$ = 6) and alveolar macrophages ($n$ = 5) after 6 h of LPS treatment. *$p \leq 0.05$, **$p \leq 0.01$, ***$p < 0.0001$.

(MABN712). Images were acquired by confocal microscopy (LSM 510 META; Zeiss) with a 63× Plan Apochromat objective lens (NA 1.4).

### *Macrophage infection and CFU assay*

*Mycobacterium smegmatis* [strain ATCC 700084/ mc(2)155] was grown in Middlebrook 7H9 medium enriched with 10% (v/v) albumin/dextrose/catalase (American Type Culture Collection) for liquid growth. Equal numbers of lung macrophages from WT and TRPML2-KO mice were plated in 24-well plates and infected with *M. smegmatis*. Following infection for 1 h, cells were washed with PBS and lysed with sterilized water. A total of 100 μl lysate was grown in LB broth. The broth was then subjected to 10-fold serial dilutions, inoculated on agar plates, and incubated at 37˚C. The number of colonies was counted (CFU) at the indicated time.

### *Cytokine array panel*

Cultured BMDMs from WT and TRPML2-KO mice were left untreated or incubated with LPS for 24 h. Cell culture supernatants were collected and centrifuged to remove particulates. A total of 100 μl supernatant was assayed immediately. To collect cell lysates, BMDMs were solubilized in lysis buffer (1% IGEPAL CA-631, 20 mM Tris-HCl [pH 8], 137 mM NaCl, 10% glycerol, 2 mM EDTA, and protease inhibitor) at 4˚C for 30 min; 25 μl cell lysate was used for the assay. Cytokine levels in BMDM supernatants and lysates were assessed using the Proteome Profiler Mouse Cytokine Array kit, Panel A (R&D Systems, Minneapolis, MN).

### *Measurement of CCL2 content in BMDM culture supernatants by ELISA*

Cell culture supernatants from WT or TRPML2$^{-/-}$ BMDMs were collected, and CCL2 was measured using an ELISA kit (R&D Systems; MJE00), per the manufacturer's instructions. Cell culture supernatants were diluted five times for the assay, and 50 μl diluted supernatant was assessed.

### *Statistics*

Groups were compared with Prism 6 software (GraphPad) using a two-tailed unpaired Student *t* test or two-way ANOVA. Data are mean ± SEM. The $p$ values $< 0.05$ were considered significant.

## Results

### *TRPML2 mRNA levels are upregulated in macrophages upon TLR activation*

To better understand TRPML2 function in a physiologically relevant cell type, we analyzed TRPML2 expression in a series of mouse tissues and organs by quantitative RT-PCR. In agreement with previous studies, we found that TRPML2 mRNA is predominantly expressed in lymphoid and kidney organs (Fig. 1A). Notably, TRPML2 expression was tightly regulated at the transcriptional

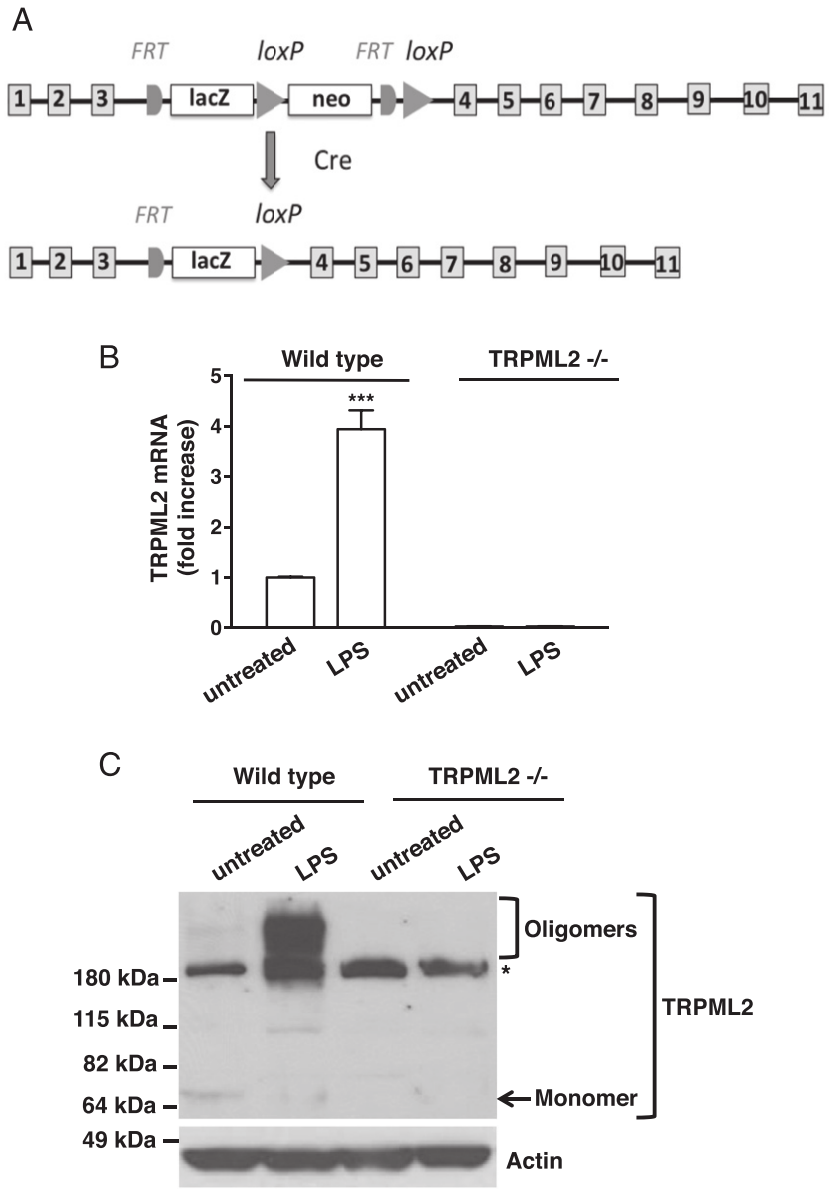


**FIGURE 2.** Generation of TRPML2-KO mice. (**A**) Schematic representation of Cre-loxP–mediated deletion of TRPML2. The KO-first allele contains a trapping cassette with a lacZ reporter and a floxed promoter-driven neo cassette inserted into the intron of the *MCOLN2* gene, thereby disrupting gene function. By crossing with the EIIA-Cre mouse, the neo cassette between two loxP sites was deleted. (**B**) BMDMs extracted from WT and TRPML2-KO mice ($n = 9$) were left untreated or incubated with LPS (1 μg/ml) for 6 h. TRPML2 mRNA levels from all groups were normalized to the WT untreated samples. Data are mRNA fold change for four independent experiments. (**C**) Primary BM macrophages from WT and KO mice were left untreated or treated with LPS (1 μg/ml) for 24 h. TRPML2 protein levels were assessed by Western blotting using rabbit anti-TRPML2 Ab. The results shown are representative of three independent experiments. The predicted molecular mass for TRPML2 is ∼65 kDa (arrow). TRPML2 oligomers run above the 180-kDa marker. The single asterisk indicates an unspecific band recognized by our Ab. Actin (42 kDa) was used as a loading control. ***$p < 0.0001$.

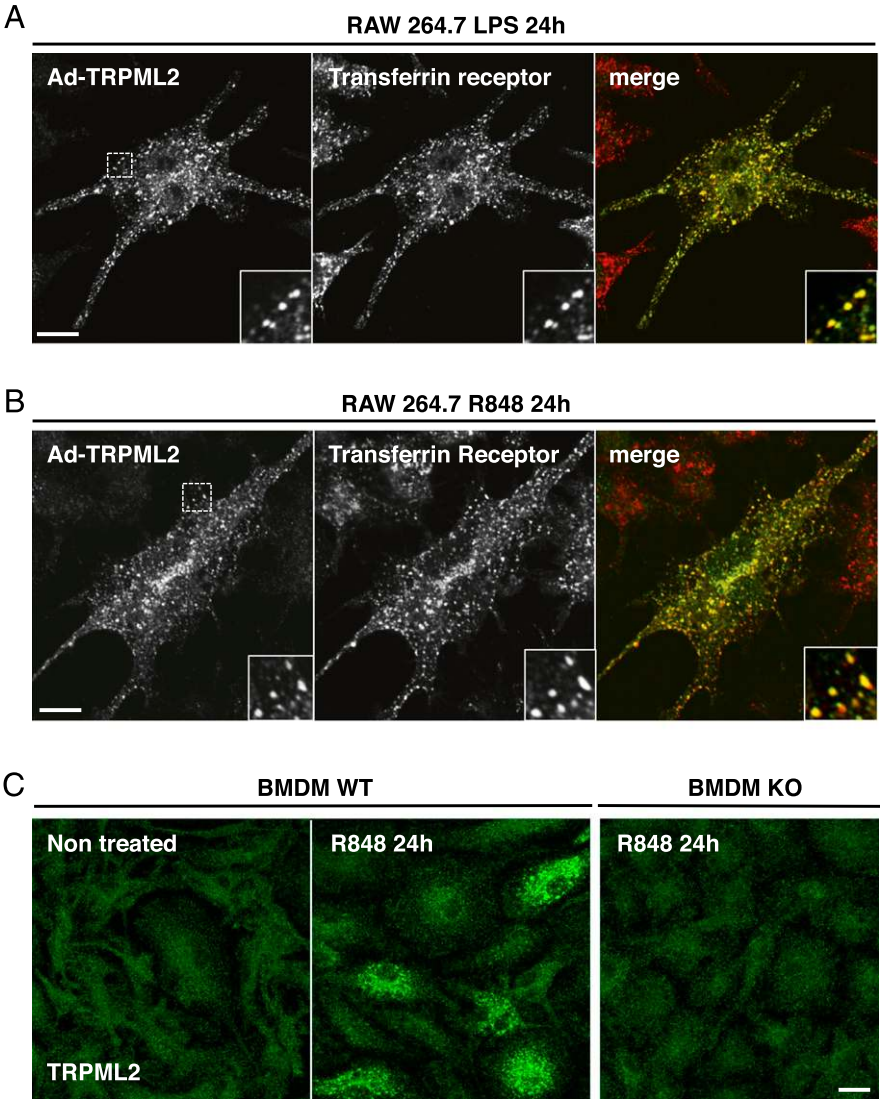


**FIGURE 3.** Intracellular distribution of TRPML2 in RAW 264.7 and BMDMs. (**A** and **B**) RAW 264.7 cells were infected with Ad-TRPML2 and stimulated with LPS (1 μg/ml) or R848 (200 ng/ml) for 24 h. Cells were permeabilized and immunostained with TRPML2 and TfR Abs and analyzed by confocal fluorescence microscopy. Yellow indicates colocalization between TRPML2 (green) and TfR (red). Images are representative of three independent experiments. *Insets* show a four-fold magnification of the indicated region. Scale bars, 10 μm. (**C**) WT and TRPML2 KO BMDMs were treated with R848 for 24 h. Endogenous TRPML2 expression was assessed using our TRPML2 Ab. Scale bar, 10 μm. Images are representative of three independent experiments.

level. Although TRPML2 was present at very low levels in resting RAW 264.7 macrophages, its expression increased >20-fold in response to LPS, an activator of TLR4 (Fig. 1B). In contrast, the mRNA levels of TRPML1 and TRPML3 did not change upon LPS stimulation (Fig. 1C).

TLRs are a family of membrane-spanning innate immune receptors that recognize ligands derived from bacteria, fungi, viruses, and parasites (32, 33). Activation of TLRs leads to a variety of downstream signals that are critical for proper immune response. To confirm upregulation of TRPML2 in response to TLR activation in primary cells, we isolated microglia cells from mice and treated them with a panel of TLR activators, including LPS (TLR4), loxoribine (TLR7), R848 (TLR7 and TLR8), and zymosan A (TLR2). In all cases, we observed an increase in the levels of TRPML2 upon TLR activation, as assessed by quantitative RT-PCR (Fig. 1D).

We then evaluated the differential expression of TRPML2 in response to various incubation times with TLR activators. This detailed kinetic analysis revealed that TRPML2 was significantly upregulated within the first 6 h of activation (Fig. 1E, 1H). In RAW 264.7 cells, TRPML2 levels reached a maximum expression 24 h after activation with either LPS or R848 and then progressively decreased back to basal levels ~72 h after activation (Fig. 1E). In contrast, maximum levels of TRPML2 mRNA expression were achieved 6 h after stimulation in a cell line of alveolar macrophages (MH-S) (Fig. 1F), as well as in primary BMDMs (Fig. 1G) and primary lung macrophages (Fig. 1H). Overall, these results show a very pronounced transcriptional upregulation of TRPML2 upon macrophage activation in both culture and primary cells.

*Generation of TRPML2-KO mice*

To characterize the role of TRPML2 in vivo, we generated TRPML2-KO mice. TRPML2-null mice were derived from an ES cell clonal cell line obtained from the Knockout Mouse Project Repository. The ES cell line contains a gene-trap cassette inserted between exons 3 and 4 of the mouse *MCOLN2* gene that results in an early truncation of the protein (Fig. 2A). Targeted disruption of TRPML2 was confirmed by quantitative RT-PCR. As seen in Fig. 2B, treatment of BMDMs with LPS for 6 h induced considerable TRPML2 expression, whereas no TRPML2 mRNA was detected in BMDMs derived from TRPML2$^{-/-}$ mice.

To further corroborate the absence of the TRPML2 protein in our KO mice, we generated a new Ab capable of detecting endogenous levels of TRPML2. In agreement with our quantitative RT-PCR analysis, we found that the levels of TRPML2 protein were almost negligible in resting BMDMs but were dramatically increased upon BMDM activation with LPS (Fig. 2C). The predicted molecular mass of mouse TRPML2 is 65 kDa. However, our Ab detected a much higher molecular mass band in activated macrophages. Several studies reported that heterologously expressed

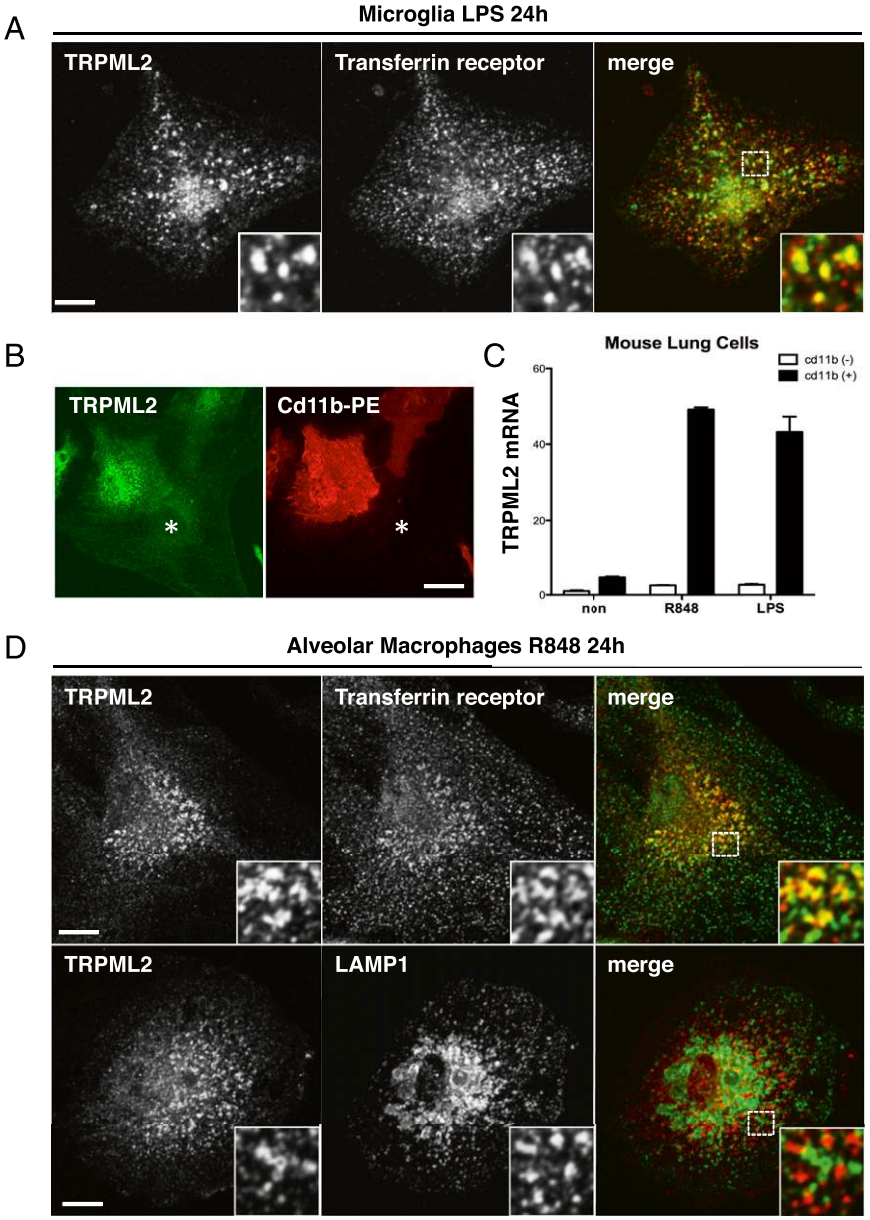


**FIGURE 4.** Endogenous TRPML2 localizes to recycling endosomes in activated microglia and alveolar macrophages. (**A**) LPS increases TRPML2 protein levels in primary mouse microglia. Primary microglia cells isolated from WT mice were treated with LPS (1 μg/ml) for 24 h. Cells were permeabilized and immunostained with TRPML2 (green) and TfR (red) Abs. *Insets* show a 4-fold magnification of the indicated region. Scale bars, 10 μm. Images are representative of three independent experiments. (**B**) Cultured primary lung cells were stimulated with R848 (200 ng/ml) for 24 h. TRPML2 expression was detected in alveolar macrophages ($CD11b^+$) but not in fibroblasts (*). Scale bar, 20 μm. (**C**) Cultured lung cells were treated with R848 (200 ng/ml) or LPS (1 μg/ml) for 10 h and sorted based on CD11b level. (**D**) Alveolar macrophages were treated with R848 (200 ng/ml) for 24 h and immunostained with TRPML2 (red) and TfR or LAMP1 (green) Abs. Yellow indicates colocalization between TRPML2 and TfR (*upper right panel*) or TRPML2 and LAMP1 (*lower right panel*). *Insets* show a 4-fold magnification of the indicated region. Scale bars, 10 μm. Images are representative of three independent experiments.

TRPML2 has the ability to form homomultimers, as well as heteromultimers, with other members of the TRPML family (34). Our results confirm that endogenous TRPML2 predominantly forms multimers in relevant cell types. As shown in Fig. 2C, there was a complete absence of TRPML2 protein in BMDMs isolated from KO mice both in resting and activation conditions.

To further confirm the specificity of our Ab, we infected ARPE-19 cells with control adenovirus or adenovirus encoding untagged mouse TRPML2 (Ad-TRPML2). As expected, our Ab detected TRPML2 monomers and oligomers in cells expressing Ad-TRPML2 but not in cells infected with control adenovirus (Supplemental Fig. 1A).

### *TRPML2 localizes to recycling endosomes in activated macrophages and microglia*

To better characterize TRPML2, we next analyzed the intracellular distribution of TRPML2 in macrophages. Expression of Ad-TRPML2 in resting or LPS-activated RAW 264.7 cells revealed that recombinant TRPML2 localized to vesicular structures dispersed throughout the cytoplasm (Fig. 3A, Supplemental Fig. 1B). Interestingly, we observed a majority of $TRPML2^+$ structures costained with the transferrin receptor (TfR), a marker of recycling endosomes (Fig. 3A, Supplemental Fig. 1B). Similar results were observed when RAW cells were activated with R848 (Fig. 3B).

To confirm the upregulation of endogenous TRPML2 in activated primary macrophages, BMDMs were incubated with R848

Table I. Analysis of kidney function in WT and TRPML2-KO mice

| | WT ($n$ = 11) | $TRPML2^{-/-}$ ($n$ = 11) |
|---|---|---|
| Blood urea nitrogen (mg/dl) | 2802 ± 231 | 2705 ± 225.6 |
| $Ca^{2+}$ (mg/dl) | 5.882 ± 0.7883 | 6.355 ± 0.3457 |
| Creatinine (mg/dl) | 57.2 ± 4.114 | 50.82 ± 4.091 |
| Glucose (mg/dl) | 49.36 ± 2.068 | 48.27 ± 2.446 |
| $Mg^{2+}$ (mg/dl) | 59.78 ± 4.336 | 57.41 ± 4.825 |
| Phosphorus (mg/dl) | 292.5 ± 26.21 | 238.6 ± 20.92 |
| $K^+$ (nmol/l) | 184.8 ± 15.81 | 182.5 ± 16.71 |
| $Na^+$ (nmol/l) | 110 ± 7.395 | 117 ± 7.469 |

Urine samples were collected from 3-mo-old female mice for urine panel analysis. WT ($n$ = 11) and KO ($n$ = 11) mouse were kept in metabolic cages for 24 h for urine collection. Data shown are mean ± SEM.

for 24 h. Treated cells were clearly stained by our anti-TRPML2 Ab, whereas no labeling was observed in untreated cells. We did not detect any positive staining in BMDMs derived from TRPML2$^{-/-}$ mice after treatment with R848, thus validating the specificity of our Ab (Fig. 3C).

Next, we aimed to corroborate the recycling endosome distribution of endogenous TRPML2 in other primary cell types. As seen in Fig. 4A, endogenous TRPML2 was detected in primary microglia when cells were treated with LPS for 24 h. Similar to RAW cells, TRPML2 localized to TfR$^{+}$ organelles. Secondly, we isolated lung tissue from WT mice. These samples included of a mix of alveolar macrophages and fibroblasts. Treatment with LPS led to TRPML2 upregulation in alveolar macrophages (CD11$^{+}$ cells) but not in fibroblasts (CD11$^{-}$ cells), as analyzed by immunofluorescence (Fig. 4B) and quantitative RT-PCR (Fig. 4C). Lastly, upregulation of TRPML2 was also observed in alveolar macrophages in response to R848 (Fig. 4C, 4D). The majority of TRPML2 vesicles colocalized with TfR (Fig. 4D). However, no colocalization with the lysosomal marker LAMP1 was observed (Fig. 4D). It is important to note that TfR cycles between recycling endosomes and the plasma membrane. Therefore, in some cells it is not unusual to find this protein both in recycling endosomes (bigger in size and concentrated in the perinuclear area) and early endosomes (smaller in size and distributed more toward the periphery of the cell). As seen in Fig. 4D, TRPML2 colocalizes with TfR almost exclusively in perinuclear endosomes. Altogether, our data show that TRPML2 colocalizes to recycling endosomes in activated macrophages and microglia.

### *Characterization of TRPML2-KO mice*

TRPML2-KO mice were obtained with a Mendelian frequency, were fertile, and had no apparent abnormalities by 20 mo of age compared with their WT counterparts. To assess growth, body weight ($n = 8$ for each genotype) was measured at regular intervals in both males and females for a period of 20 wk and then again at 78 wk. The body weight of TRPML2$^{-/-}$ mice was not different from that of control mice (Supplemental Fig. 2).

At 3 and 18 mo of age, control and TRPML2$^{-/-}$ mice were compared using several tests designed to assess muscle, cerebellar, sensory, and neuropsychiatric function. These included SHIRPA (SmithKline Beecham, Harwell, Imperial College, Royal London Hospital, phenotype assessment), open field test, gait analysis, grip strength and rotarod, and modified Morris water test. No significant differences were observed between control and KO mice (data not shown).

Because of the relatively high levels of expression of TRPML2 in kidney (Fig. 1A), control and KO mice were placed in metabolic cages, and renal function was assessed. Table I summarizes the metabolic cage data obtained and shows that there were no significant differences in baseline values for the examined parameters between WT and TRPML2-KO mice.

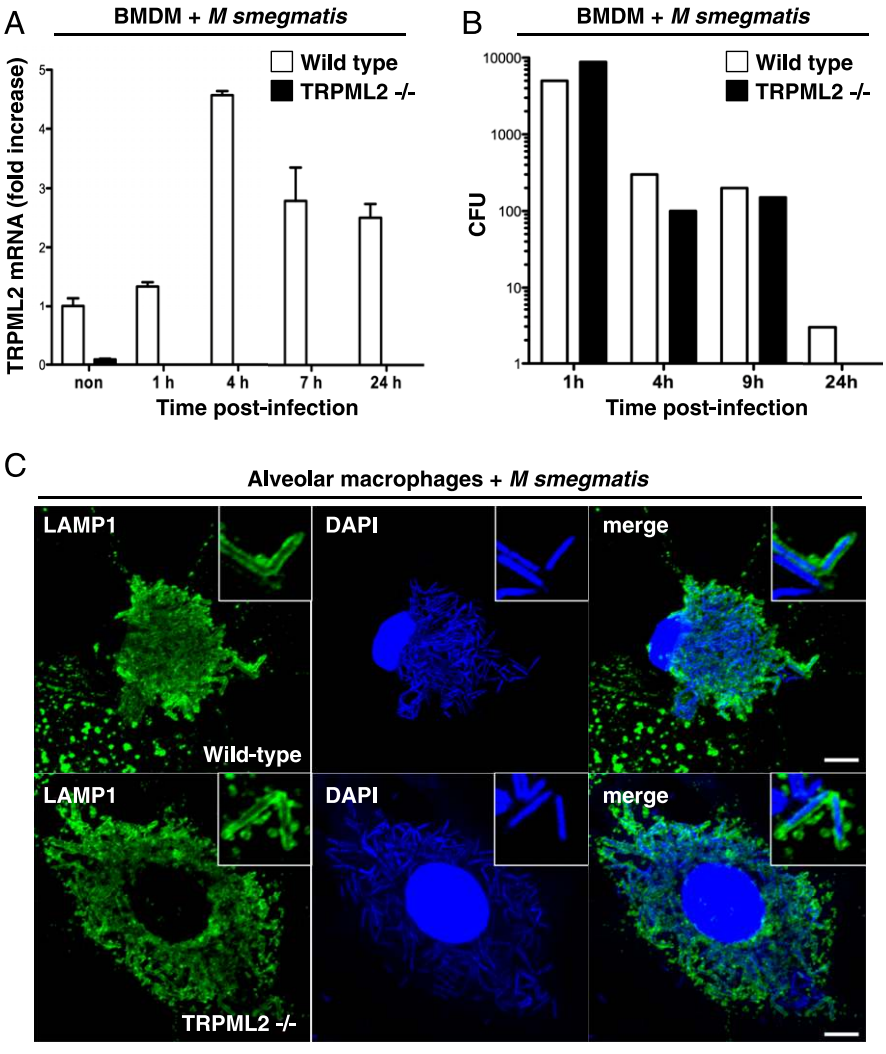


**FIGURE 5.** *M. smegmatis* degradation in alveolar macrophages does not require TRPML2. (**A**) *M. smegmatis* infection induced TRPML2 mRNA levels in BMDMs derived from WT mice. Equal numbers of macrophages from WT and TRPML2-KO mice were plated and infected with the same amount of *M. smegmatis*. Cells were collected at the indicated time points, and TRPML2 mRNA was measured by RT-PCR. (**B**) The efficiency of WT and TRPML2-KO BMDMs with regard to the elimination of engulfed *M. smegmatis* was measured as CFU. Cultured BMDMs were infected with *M. smegmatis* at a 1:100 ratio (multiplicity of infection = 100). Infected macrophages were lysed at the indicated time points. Cell lysates were resuspended in 800 μl of LB broth and subjected to serial dilution. Ten microliters of each dilution was plated on LB agar plates. After overnight incubation, the numbers of bacterial colonies were counted. (**C**) Infected alveolar macrophages were fixed and stained with LAMP1 Ab (green) and DAPI (blue). The *insets* show tubular lysosomes surrounding *M. smegmatis* in WT (*upper panels*) and KO (*lower panels*) macrophages. *Insets* show a 4-fold magnification of the indicated region. Scale bars, 5 μm. Images are representative of three independent experiments.

*Altered chemokine secretion in TRPML2$^{-/-}$ mice*

The strong transcriptional upregulation of TRPML2 in activated macrophages suggests that TRPML2 might have an important role in the regulation of macrophage activation or function. To address this possibility, BMDMs from control and TRPML2$^{-/-}$ mice were treated with LPS for different periods of time. No significant difference in the surface levels of F4/80, CD80, or MHC class I was observed between control and TRPML2$^{-/-}$ cells, suggesting that TRPML2 is not required for the trafficking of these proteins to the plasma membrane (Supplemental Fig. 3).

It was reported that CG8743, the homolog of TRPMLs in *Drosophila melanogaster*, plays a role in restricting growth of *M. smegmatis* in S2 cells, likely by facilitating delivery of the bacteria to lysosomes and subsequent degradation (35). Therefore, we checked whether TRPML2 might play an analogous role to CG8743 in mouse macrophages. Infection of BMDMs isolated from control mice with *M. smegmatis* substantially induced TRPML2 expression that was maximal at 4 h postinfection (Fig. 5A). This suggested that TRPML2 upregulation occurs not only in response to purified TLR ligands but also to live bacteria. However, when analyzed by CFU, there was no difference in bacterial uptake or growth between control and TRPML2$^{-/-}$ cells; and, most bacteria were degraded after 24 h (Fig. 5B). Moreover, we observed *M. smegmatis* delivery to lysosomes in alveolar macrophages isolated from both control and KO mice (Fig. 5C). Therefore, it is possible that another member of the TRPML family, most likely TRPML1, accounts for the degradation defect reported in *drosophila* S2 cells (18).

To better understand the potential role of TRPML2 in the immune response, we measured cytokine and chemokine production using commercially available Ab arrays. BMDMs isolated from WT or TRPML2$^{-/-}$ mice were treated with LPS for 24 h. Cell lysates were collected and incubated with nitrocellulose membranes in which Abs for 40 cytokines and chemokines had been spotted (cytokine array panels). Interestingly, we found that the levels of specific chemokines (CCL3, CCL5, and CXCL2), as well as the intracellular adhesion molecule-1 (or CD54), were reduced in samples obtained from TRPML2-KO animals (Fig. 6A). This reduction was very consistent when the experiments were repeated using different pairs of WT and KO animals (Fig. 6B). In addition, we performed a time-course analysis of LPS activation and found that the amount of secreted CCL2 (measured by ELISA) was significantly decreased in TRPML2$^{-/-}$ cell culture supernatants at all time points (Fig. 6C). Similar results were obtained by incubating cell supernatants from LPS-treated WT and TRPML2$^{-/-}$ BMDMs with cytokine array panels (Fig. 6D). The reduction in the levels of specific chemokines was not the result of failed induction, because the transcriptional upregulation of CCL5, CCL3, and CCL2 was not significantly different between WT and TRPML2$^{-/-}$ mice following LPS treatment (Supplemental Fig. 4).

These results suggest that TRPML2 might play a role in the regulation of trafficking and/or secretion. In agreement with this idea, we found increased accumulation of CCL2 in the Golgi of

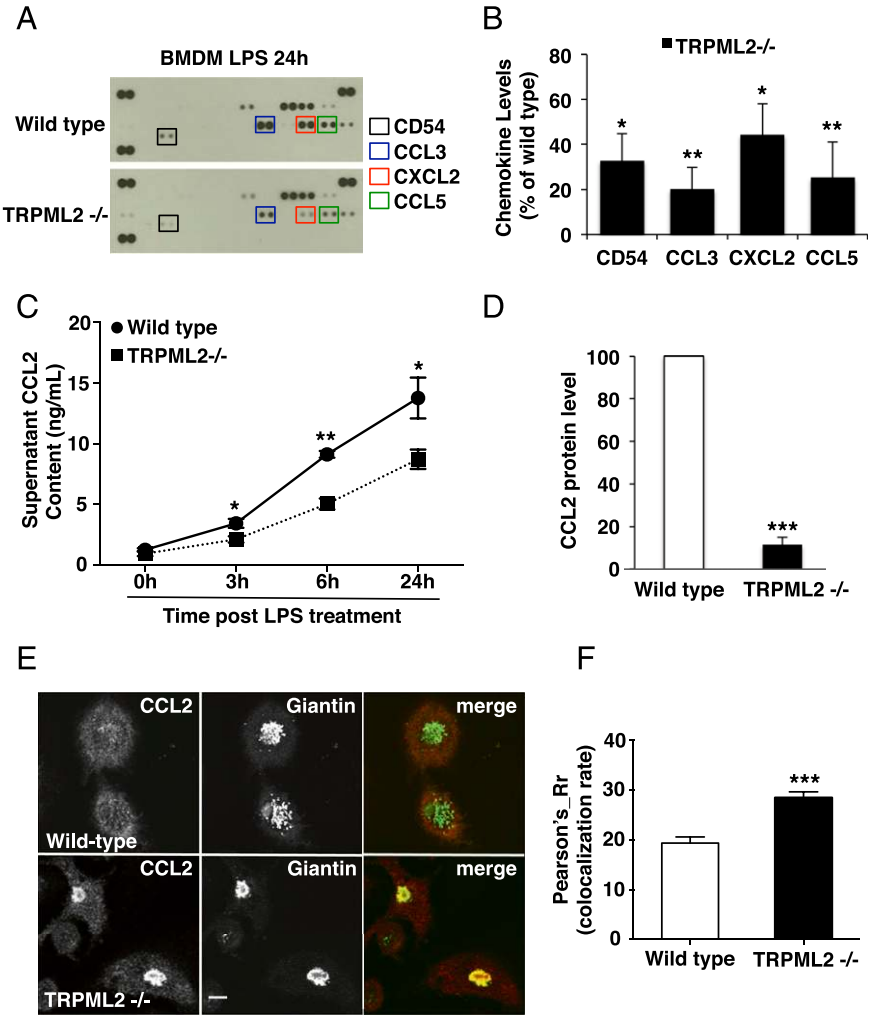


**FIGURE 6.** Chemokine secretion is reduced in TRPML2-KO mice. (**A**) BMDMs from WT and TRPML2-KO mice were treated with LPS for 24 h. Cell lysates were extracted and analyzed using the Proteome Profiler Mouse Cytokine Array (R&D Systems). Blots are representative of three independent experiments. (**B**) Spot intensities from the blots in (A) were quantified using ImageJ. Data are percentage change (mean ± SEM) in lysate cytokine levels in TRPML2-KO mice compared with WT mice of three independent experiments. *$p \leq 0.01$, **$p \leq 0.001$, Student *t* test. (**C**) BMDMs from WT and TRPML2-KO mice were treated with LPS for the indicated times. The CCL2 content in cell supernatants was analyzed by ELISA. Data are mean ± SEM of five independent experiments. *$p \leq 0.05$, **$p \leq 0.005$, Student *t* test. (**D**) BMDMs from WT and TRPML2-KO mice were treated with LPS for 24 h. The cytokine content in culture supernatants was analyzed as in (A). Data are percentage change (mean ± SEM) in serum cytokine levels in TRPML2-KO mice compared with WT mice of three independent experiments. ***$p \leq 0.0005$, Student *t* test. (**E**) BMDMs isolated from WT and TRPML2-KO mice were treated with LPS (1 μg/ml) for 24 h. Cells were permeabilized and immunostained with CCL2 (red) and giantin (green) Abs. Scale bar, 10 μm. Images are representative of three independent experiments. (**F**) Colocalization between CCL2 and giantin in LPS-treated WT ($n = 154$) and TRPML2$^{-/-}$ ($n = 169$) BMDMs was quantified using the Pearson coefficient. ***$p \leq 0.005$.

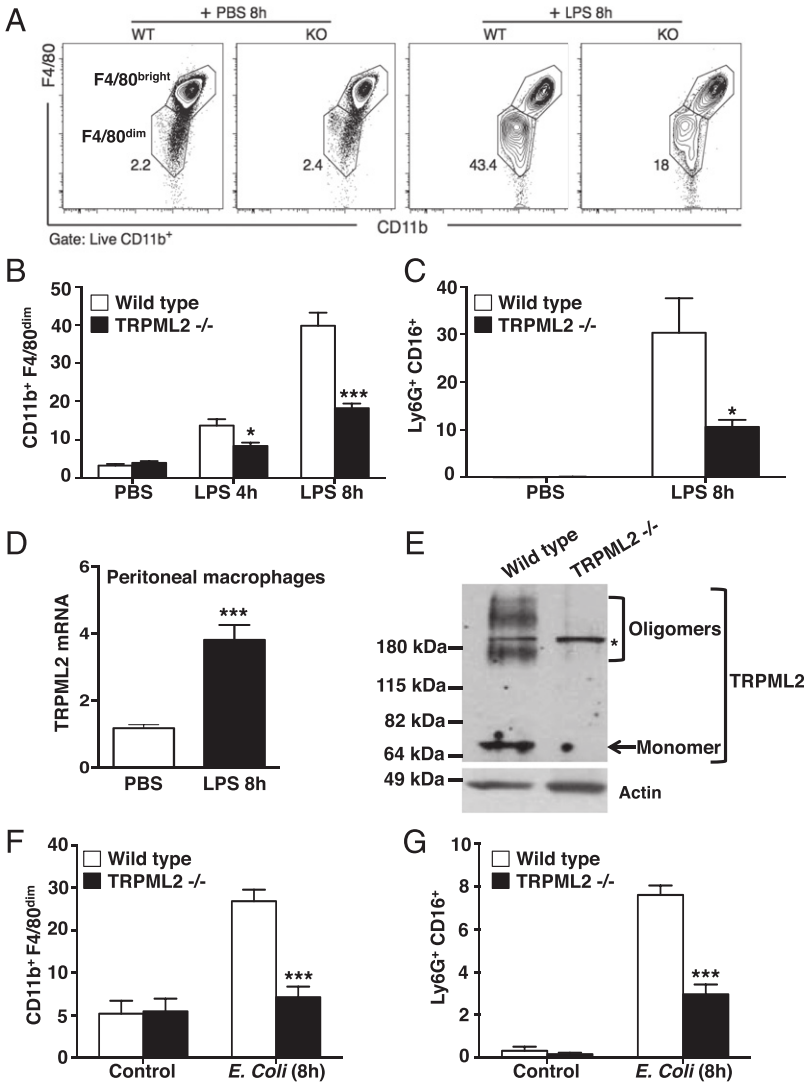


**FIGURE 7.** Macrophage migration is impaired in TRPML2-KO mice. (**A**) Flow cytometric analysis of $CD11b^+F4/80^{bright}$ (indicative of resident macrophages) and $CD11b^+F4/80^{dim}$ (indicative of recruited macrophages) peritoneal macrophages isolated from peritoneal fluid of WT and TRPML2-KO mice injected with saline or LPS for 8 h. Numbers represent the percentage of $CD11b^+F4/80^{dim}$ cells among $CD11b^+$ cells. (**B**) Percentage of $CD11b^+F4/80^{dim}$ cells from WT and TRPML2-KO mice injected with saline or LPS (0.5 μg/g) for 4 or 8 h. Data are mean ± SD of at least three independent experiments (LPS 4 h: $n = 4$, LPS 8 h: $n = 16$, saline: $n = 11$). $^*p < 0.05$, $^{***}p < 0.0005$, two-way ANOVA. (**C**) Percentage of neutrophils ($Ly6G^+CD16^+$ cells) from WT and TRPML2-KO mice injected with saline or LPS (0.5 μg/g) for 8 h. Data are mean ± SD of three independent experiments (LPS 8 h: $n = 7$, saline: $n = 5$). $^*p < 0.05$, two-way ANOVA. (**D**) TRPML2 mRNA levels from peritoneal macrophages isolated from WT mice that were injected with saline or LPS. Error bars represent SEM (LPS: $n = 13$, saline: $n = 7$). $^{***}p < 0.0001$, two-tailed unpaired Student $t$ test. (**E**) TRPML2 protein levels in peritoneal macrophages extracted from WT and KO mouse were assessed by Western blot. The predicted molecular mass for TRPML2 is ~65 kDa (arrow). TRPML2 oligomers run above the 180-kDa marker. The single asterisk indicates an unspecific band recognized by our Ab. Actin (42 kDa) was used as a loading control. The image shown is a representative from three independent experiments. (**F**) Percentage of $CD11b^+F4/80^{dim}$ cells from WT and TRPML2-KO mice injected with saline or live ETEC (strain H10407) ($5 \times 10^7$ CFU) for 8 h. Data are mean ± SD of two independent experiments (*E. coli*: $n = 5$, saline: $n = 3$). $^{***}p < 0.0005$, two-way ANOVA. (**G**) Percentage of $Ly6G^+CD16^+$ cells from WT and TRPML2-KO mice injected with saline or live ETEC (strain H10407) ($5 \times 10^7$ CFU) for 8 h. Data are mean ± SD of two independent experiments (*E. coli*: $n = 5$, saline: $n = 3$). $^{***}p < 0.0005$, two-way ANOVA.

LPS-treated $TRPML2^{-/-}$ BMDMs compared with WT cells (Fig. 6E). Analysis of >150 randomly selected cells using the Pearson coefficient revealed that the increased colocalization of CCL2 with the Golgi marker Giantin observed in $TRPML2^{-/-}$ cells was statistically significant (Fig. 6F). Altogether, our data revealed that trafficking of specific chemokines is significantly altered in $TRPML2^{-/-}$ macrophages.

### *In vivo migration of macrophages is impaired in the absence of TRPML2*

Chemokines, in particular CCL2, play a critical role in promoting infiltration and migration of monocytes and macrophages to the sites of inflammation (36). To determine whether the migration of macrophages was altered in TRPML2-KO mice, we evaluated in vivo recruitment of peripheral macrophages in response to i.p. injections of LPS. Eight hours after LPS injection, cells were collected from the peritoneum and labeled for the macrophage marker F4/80. $F4/80^+$ cells were separated into two populations, dim and bright, which were shown to be indicative of recruited and resident macrophages, respectively (Fig. 7A) (37). Notably, macrophage recruitment in response to LPS was markedly reduced in TRPML2-KO mice (Fig. 7B). In contrast, the number of resident macrophages was comparable between control and KO mice (data not shown). Migration of neutrophils to the intraperitoneal space was also significantly decreased in $TRPML2^{-/-}$ animals (Fig. 7C). Measurement of TRPML2 mRNA and protein levels in peritoneal macrophages confirmed upregulation of TRPML2 in response to LPS in vivo (Fig. 7D, 7E).

To further confirm the physiological relevance of our observations, we injected mice i.p. with live ETEC strain H10407 and measured migration of macrophages and neutrophils into the i.p. space at 8 h after the administration of the live bacteria. As expected, we found a very significant delay in both macrophage and neutrophil migration in $TRPML2^{-/-}$ animals (Fig. 7F, 7G). Altogether, out data reveal a novel role for TRPML2 in the regulation of the innate immune response.

## Discussion

To our knowledge, this is the first description of a role for TRPML2 in the immune response. TRPML2 mRNA and protein levels were dramatically upregulated in culture and primary macrophages upon TLR activation. The increased expression of TRPML2 upon activation of different TLRs indicates that it might participate in the host defense against different types of microbial pathogens, including bacteria (recognized by TLR4) and viruses (recognized by TLR7 and TLR8). Recent evidence suggests that the expression of other TRPMLs may also be regulated at the transcriptional level. TRPML1 is upregulated following activation of transcription factor EB (TFEB) and transcription factor E3 (TFE3) (38, 39). TFEB and TFE3 translocate to the nucleus upon

nutrient deprivation and induce the expression of a complex gene network, leading to autophagy activation and lysosomal biogenesis (40). It was proposed that the increased levels of TRPML1 in response to TFEB/TFE3 activation are critical in facilitating fusion of autophagosomes with lysosomes and, in some cases, may also mediate fusion of lysosomes with the plasma membrane (20). Likewise, TRPML3 is highly expressed in neonatal enterocytes, where it plays an important role in the digestion of maternal-provided nutrients by regulating fusion/fission events between late endosomes/lysosomes, whereas it is absent in mature intestinal enterocytes (25).

Most studies addressing the intracellular distribution of TRPMLs relied upon overexpression of recombinant proteins. The low TRPML expression in basal conditions may explain the difficulty of generating Abs capable of detecting endogenous protein levels. Our results suggest that visualization of endogenous TRPMLs may require analyzing specific cell types or activation conditions. For example, we described earlier that heterologously expressed TRPML2 localized primarily to recycling endosomes in HeLa cells. However, under these conditions, some TRPML2$^{+}$ staining was also observed at the plasma membrane and lysosomes. The extensive colocalization with TfR reveals that, at least in activated macrophages and microglia, endogenous TRPML2 distributes almost exclusively to recycling endosomes. In addition, it was suggested that TRPML1 and TRPML3, both of which localize to early/late endosomal compartments, might be redundant in some cell types (25). The distinct distribution of TRPML2 in recycling endosomes argues against a possible redundancy between TRPML2 and the other members of the TRPML family.

Work from several laboratories supports the concept that TRPMLs function as calcium release channels that regulate fusion of endosomal organelles with different cellular compartments. In agreement with this idea, we described earlier that, in HeLa cells, TRPML2 facilitates trafficking of certain proteins along the recycling pathway (31). Therefore, we propose that increased expression of TRPML2 in activated macrophages might lead to more dynamic vesicular carriers, thus increasing membrane fusion and enhancing protein recycling and/or secretion. Accordingly, we found increased intracellular accumulation and reduced secretion of CCL2 in BMDMs isolated from TRPML2-KO mice. Chemokine/cytokine secretion does not follow a unique trafficking pathway, but rather could involve multiple pathways and organelles depending on whether they get delivered locally or whether the release is more multidirectional on the cell surface. For example, in macrophages, IL-6 and TNF reside in distinct nonoverlapping areas of recycling endosomes, suggesting that this compartment may function as a sorting hub for local secretion of cytokines (41). Moreover, in mast cells, CCL2 secretion is inhibited by inactivation of syntaxin 6, a *t*-SNARE required for fusion of vesicular carriers arriving from the *trans*-Golgi network to recycling endosomes (42). Therefore, TRPML2 could facilitate fusion of recycling endosomes with either *trans*-Golgi network–derived carriers or plasma membrane, thus promoting secretion of specific chemokines/cytokines.

It is well established that CCL2 promotes attraction of immune cells to the sites of inflammation. Although we cannot rule out additional defects in TRPML2$^{-/-}$ macrophages, the reduced levels of CCL2 and other migratory chemokines are consistent with the decreased numbers of recruited macrophages observed in vivo. In fact, mice deficient in CCL2 receptor show delayed recruitment of F4/80$^{dim}$ macrophages to the lungs upon *Mycobacterium tuberculosis* infection (37). Future studies should address the susceptibility of TRPML2-KO mice to *M. tuberculosis* and other pathogens.

In summary, our work reveals a novel and exciting role for TRPML2 in the regulation of the innate immune response. It also suggests that cells may regulate expression of TRPMLs in response to specific stimuli as a way to enhance specific trafficking pathways.

## Acknowledgments

We thank Dr. Chengyu Liu and Dr. Danielle Springer (NHLBI Transgenic and Murine Phenotyping Cores, respectively) for assistance.

## Disclosures

The authors have no financial conflicts of interest.

## References

1. Abe, K., and R. Puertollano. 2011. Role of TRP channels in the regulation of the endosomal pathway. *Physiology (Bethesda)* 26: 14–22.
2. Venkatachalam, K., and C. Montell. 2007. TRP channels. *Annu. Rev. Biochem.* 76: 387–417.
3. Puertollano, R., and K. Kiselyov. 2009. TRPMLs: in sickness and in health. *Am. J. Physiol. Renal Physiol.* 296: F1245–F1254.
4. Venkatachalam, K., C. O. Wong, and M. X. Zhu. 2015. The role of TRPMLs in endolysosomal trafficking and function. *Cell Calcium* 58: 48–56.
5. Bargal, R., N. Avidan, E. Ben-Asher, Z. Olender, M. Zeigler, A. Frumkin, A. Raas-Rothschild, G. Glusman, D. Lancet, and G. Bach. 2000. Identification of the gene causing mucolipidosis type IV. *Nat. Genet.* 26: 118–123.
6. Bassi, M. T., M. Manzoni, E. Monti, M. T. Pizzo, A. Ballabio, and G. Borsani. 2000. Cloning of the gene encoding a novel integral membrane protein, mucolipidin-and identification of the two major founder mutations causing mucolipidosis type IV. *Am. J. Hum. Genet.* 67: 1110–1120.
7. Slaugenhaupt, S. A., J. S. Acierno, Jr., L. A. Helbling, C. Bove, E. Goldin, G. Bach, R. Schiffmann, and J. F. Gusella. 1999. Mapping of the mucolipidosis type IV gene to chromosome 19p and definition of founder haplotypes. *Am. J. Hum. Genet.* 65: 773–778.
8. Altarescu, G., M. Sun, D. F. Moore, J. A. Smith, E. A. Wiggs, B. I. Solomon, N. J. Patronas, K. P. Frei, S. Gupta, C. R. Kaneski, et al. 2002. The neurogenetics of mucolipidosis type IV. *Neurology* 59: 306–313.
9. Amir, N., J. Zlotogora, and G. Bach. 1987. Mucolipidosis type IV: clinical spectrum and natural history. *Pediatrics* 79: 953–959.
10. Berman, E. R., N. Livni, E. Shapira, S. Merin, and I. S. Levij. 1974. Congenital corneal clouding with abnormal systemic storage bodies: a new variant of mucolipidosis. *J. Pediatr.* 84: 519–526.
11. Livni, N., and C. Legum. 1976. Ultrastructure of cultured fibroblasts in mucolipidosis type IV. *Exp. Cell Biol.* 44: 1–11.
12. Tellez-Nagel, I., I. Rapin, T. Iwamoto, A. B. Johnson, W. T. Norton, and H. Nitowsky. 1976. Mucolipidosis IV. Clinical, ultrastructural, histochemical, and chemical studies of a case, including a brain biopsy. *Arch. Neurol.* 33: 828–835.
13. Di Palma, F., I. A. Belyantseva, H. J. Kim, T. F. Vogt, B. Kachar, and K. Noben-Trauth. 2002. Mutations in Mcoln3 associated with deafness and pigmentation defects in varitint-waddler (Va) mice. *Proc. Natl. Acad. Sci. USA* 99: 14994–14999.
14. Pryor, P. R., F. Reimann, F. M. Gribble, and J. P. Luzio. 2006. Mucolipin-1 is a lysosomal membrane protein required for intracellular lactosylceramide traffic. *Traffic* 7: 1388–1398.
15. Thompson, E. G., L. Schaheen, H. Dang, and H. Fares. 2007. Lysosomal trafficking functions of mucolipin-1 in murine macrophages. *BMC Cell Biol.* 8: 54.
16. Vergarajauregui, S., and R. Puertollano. 2006. Two di-leucine motifs regulate trafficking of mucolipin-1 to lysosomes. *Traffic* 7: 337–353.
17. Vergarajauregui, S., P. S. Connelly, M. P. Daniels, and R. Puertollano. 2008. Autophagic dysfunction in mucolipidosis type IV patients. *Hum. Mol. Genet.* 17: 2723–2737.
18. Samie, M., X. Wang, X. Zhang, A. Goschka, X. Li, X. Cheng, E. Gregg, M. Azar, Y. Zhuo, A. G. Garrity, et al. 2013. A TRP channel in the lysosome regulates large particle phagocytosis via focal exocytosis. *Dev. Cell* 26: 511–524.
19. LaPlante, J. M., M. Sun, J. Falardeau, D. Dai, E. M. Brown, S. A. Slaugenhaupt, and P. M. Vassilev. 2006. Lysosomal exocytosis is impaired in mucolipidosis type IV. *Mol. Genet. Metab.* 89: 339–348.
20. Medina, D. L., A. Fraldi, V. Bouche, F. Annunziata, G. Mansueto, C. Spampanato, C. Puri, A. Pignata, J. A. Martina, M. Sardiello, et al. 2011. Transcriptional activation of lysosomal exocytosis promotes cellular clearance. *Dev. Cell* 21: 421–430.
21. Soyombo, A. A., S. Tjon-Kon-Sang, Y. Rbaibi, E. Bashllari, J. Bisceglia, S. Muallem, and K. Kiselyov. 2006. TRP-ML1 regulates lysosomal pH and acidic lysosomal lipid hydrolytic activity. *J. Biol. Chem.* 281: 7294–7301.
22. Dong, X. P., X. Cheng, E. Mills, M. Delling, F. Wang, T. Kurz, and H. Xu. 2008. The type IV mucolipidosis-associated protein TRPML1 is an endolysosomal iron release channel. *Nature* 455: 992–996.
23. Kukic, I., J. K. Lee, J. Coblentz, S. L. Kelleher, and K. Kiselyov. 2013. Zinc-dependent lysosomal enlargement in TRPML1-deficient cells involves MTF-1 transcription factor and ZnT4 (Slc30a4) transporter. *Biochem. J.* 451: 155–163.
24. Castiglioni, A. J., N. N. Remis, E. N. Flores, and J. García-Añoveros. 2011. Expression and vesicular localization of mouse Trpml3 in stria vascularis, hair

cells, and vomeronasal and olfactory receptor neurons. *J. Comp. Neurol.* 519: 1095–1114.
25. Remis, N. N., T. Wiwatpanit, A. J. Castiglioni, E. N. Flores, J. A. Cantú, and J. García-Añoveros. 2014. Mucolipin co-deficiency causes accelerated endolysosomal vacuolation of enterocytes and failure-to-thrive from birth to weaning. *PLoS Genet.* 10: e1004833.
26. Kim, H. J., A. A. Soyombo, S. Tjon-Kon-Sang, I. So, and S. Muallem. 2009. The Ca(2+) channel TRPML3 regulates membrane trafficking and autophagy. *Traffic* 10: 1157–1167.
27. Martina, J. A., B. Lelouvier, and R. Puertollano. 2009. The calcium channel mucolipin-3 is a novel regulator of trafficking along the endosomal pathway. *Traffic* 10: 1143–1156.
28. Lelouvier, B., and R. Puertollano. 2011. Mucolipin-3 regulates luminal calcium, acidification, and membrane fusion in the endosomal pathway. *J. Biol. Chem.* 286: 9826–9832.
29. Lev, S., D. A. Zeevi, A. Frumkin, V. Offen-Glasner, G. Bach, and B. Minke. 2010. Constitutive activity of the human TRPML2 channel induces cell degeneration. *J. Biol. Chem.* 285: 2771–2782.
30. Samie, M. A., C. Grimm, J. A. Evans, C. Curcio-Morelli, S. Heller, S. A. Slaugenhaupt, and M. P. Cuajungco. 2009. The tissue-specific expression of TRPML2 (MCOLN-2) gene is influenced by the presence of TRPML1. *Pflugers Arch.* 459: 79–91.
31. Karacsonyi, C., A. S. Miguel, and R. Puertollano. 2007. Mucolipin-2 localizes to the Arf6-associated pathway and regulates recycling of GPI-APs. *Traffic* 8: 1404–1414.
32. Beutler, B. 2004. Inferences, questions and possibilities in Toll-like receptor signalling. *Nature* 430: 257–263.
33. Janssens, S., and R. Beyaert. 2003. Role of Toll-like receptors in pathogen recognition. *Clin. Microbiol. Rev.* 16: 637–646.
34. Venkatachalam, K., T. Hofmann, and C. Montell. 2006. Lysosomal localization of TRPML3 depends on TRPML2 and the mucolipidosis-associated protein TRPML1. *J. Biol. Chem.* 281: 17517–17527.
35. Philips, J. A., M. C. Porto, H. Wang, E. J. Rubin, and N. Perrimon. 2008. ESCRT factors restrict mycobacterial growth. *Proc. Natl. Acad. Sci. USA* 105: 3070–3075.
36. Bose, S., and J. Cho. 2013. Role of chemokine CCL2 and its receptor CCR2 in neurodegenerative diseases. *Arch. Pharm. Res.* 36: 1039–1050.
37. Peters, W., J. G. Cyster, M. Mack, D. Schlöndorff, A. J. Wolf, J. D. Ernst, and I. F. Charo. 2004. CCR2-dependent trafficking of F4/80dim macrophages and CD11cdim/intermediate dendritic cells is crucial for T cell recruitment to lungs infected with *Mycobacterium tuberculosis*. *J. Immunol.* 172: 7647–7653.
38. Martina, J. A., H. I. Diab, L. Lishu, L. Jeong-A, S. Patange, N. Raben, and R. Puertollano. 2014. The nutrient-responsive transcription factor TFE3 promotes autophagy, lysosomal biogenesis, and clearance of cellular debris. *Sci. Signal.* 7: ra9.
39. Sardiello, M., M. Palmieri, A. di Ronza, D. L. Medina, M. Valenza, V. A. Gennarino, C. Di Malta, F. Donaudy, V. Embrione, R. S. Polishchuk, et al. 2009. A gene network regulating lysosomal biogenesis and function. *Science* 325: 473–477.
40. Settembre, C., C. Di Malta, V. A. Polito, M. Garcia Arencibia, F. Vetrini, S. Erdin, S. U. Erdin, T. Huynh, D. Medina, P. Colella, et al. 2011. TFEB links autophagy to lysosomal biogenesis. *Science* 332: 1429–1433.
41. Manderson, A. P., J. G. Kay, L. A. Hammond, D. L. Brown, and J. L. Stow. 2007. Subcompartments of the macrophage recycling endosome direct the differential secretion of IL-6 and TNFalpha. *J. Cell Biol.* 178: 57–69.
42. Frank, S. P., K. P. Thon, S. C. Bischoff, and A. Lorentz. 2011. SNAP-23 and syntaxin-3 are required for chemokine release by mature human mast cells. *Mol. Immunol.* 49: 353–358.